Direct Probing of Schottky Barriers in Si Nanowire Schottky Barrier Field Effect Transistors

Dominik Martin,[1,*] Andre Heinzig,[1] Matthias Grube,[1] Lutz Geelhaar,[2] Thomas Mikolajick,[1,3] Henning Riechert,[2] and Walter M. Weber[1]

[1]*Namlab gGmbH, 01187 Dresden, Germany*

[2]*Paul-Drude-Institut für Festkörperelektronik, 10117 Berlin, Germany*

[3]*Chair of Nanoelectronic Materials, Technische Universität Dresden, 01062 Dresden, Germany*

(Received 5 July 2011; published 18 November 2011)

This work elucidates the role of the Schottky junction in the electronic transport of nanometer-scale transistors. In the example of Schottky barrier silicon nanowire field effect transistors, an electrical scanning probe technique is applied to examine the charge transport effects of a nanometer-scale local top gate during operation. The results prove experimentally that Schottky barriers control the charge carrier transport in these devices. In addition, a proof of concept for a reprogrammable nonvolatile memory device based on band bending at the Schottky barriers will be shown.

DOI: 10.1103/PhysRevLett.107.216807 PACS numbers: 85.35.−p, 62.23.Hj, 73.63.Rt

Complementary metal oxide semiconductor devices rely on the combination of *n*- and *p*-type field effect transistors (FETs). These in turn rely on the *n*- and *p*-type doping of the different regions within the transistors. The exact control of the doping level becomes increasingly difficult as scaling progresses to smaller feature sizes. Moreover, semiconductor size and choice of surrounding materials have a significant influence on the activation of free charge carriers from dopant atoms in nanometer-scale semiconductors [1,2]. Schottky field effect transistors (SBFETs) were first proposed by Nishi and Sze, by replacing the heavily doped source and drain region of a conventional FET with metal electrodes, while remaining fully compliant with established complementary metal oxide semiconductor processing technology [3,4]. Over the past decade, the investigation of the transport properties of nanometer-scale Schottky transistors made of carbon nanotubes, graphene, and semiconductor nanowires has attracted increasing attention [5–8]. The charge transport behavior strongly differs from that of conventional FETs, especially in the on- and subthreshold regions [9]. In the on state, injection through the source Schottky junction becomes the limiting factor. In the transfer characteristics ($I_d - V_g$) the subthreshold region can be generally subdivided into two regions: current injection dominated by thermionic emission over the energy barrier at low electric gate fields and currents dominated by tunneling at high fields (thin barriers) [10]. It has been shown that scaling down the Schottky junction dimensions and semiconductor body thickness significantly enhances the tunneling current [11–13]. They are being studied extensively as building blocks for future electronic applications such as reprogrammable devices and biosensors [8,14]. The broad range of electronic properties unique to nanowires has recently led to the development of nanowire-based Boolean logic devices [15–17]. Specifically, metal-semiconductor axial nanowire (NW) heterostructures exhibit an optimal geometry for enhancing tunneling at the Schottky electrodes [18]. Although these devices have been investigated for some time, direct experimental proof that carrier injection at the Schottky barrier limits the entire NW transport has been missing. In order to understand the working principle of SiNWSBFETs, it is of immense interest to study the charge carrier transport at the Schottky junctions. In this respect atomic force microscopy (AFM) and scanning gate microscopy (SGM) are powerful and established tools to characterize the charge carrier transport in nanodevices [19–22]. Freitag *et al.* have already imaged Schottky barriers in carbon nanotube FETs by SGM. This experiment combines a working undoped SiNWSBFET with an electrical scanning probe technique to examine the effects of a nanoscale and mobile top gate on a back-gated SiNWSBFET during operation. We will deliver direct experimental proof that the Schottky barriers control the charge carrier transport in SiNWSBFET. Additional experiments show that nonvolatile programming is possible at the Schottky junction.

The SiNWSBFET's core is composed of metal/Si/metal axial NW heterostructures. Such heterostructures were synthesized by a bottom-up approach. Undoped Si nanowires were grown epitaxially by chemical vapor deposition using the vapor liquid solid method, employing Au particles [14,23,24]. The metallic segments are chosen to be $NiSi_2$ and act as the source and drain. These were fabricated by the thermally activated axial intrusion of nickel silicides into the Si NW from prepatterned Ni reservoirs [24]. This creates two abrupt Schottky junctions within the NW [8,24,25]. Both Si and $NiSi_2$ parts of the NW are coated with an approximately 2 nm thick native SiO_2. These Schottky junctions can be probed individually by SGM using a conductive AFM tip to bend the conduction and valence bands locally at the metal-semiconductor junction. The SGM used in this work is an AFM operated in contact mode, where two probe tip micromanipulators

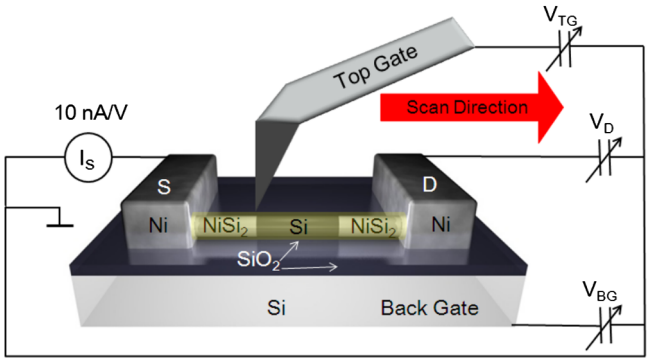

FIG. 1 (color online). Schematic of the SGM setup. The $NiSi_2$ electrodes act as the source and drain. The Si substrate is the back gate, and the conductive AFM Tip is the scanning top gate.

are positioned under the AFM head along with the conductive AFM tip. One probe contacts the source, and the other the drain electrode. The conductive tip also acts as a local top gate. Consequently, the source current I_S is measured in dependence of the top gate position, by scanning across the nanowire surface at a fixed top gate V_{TG} and drain V_D bias. To simplify the upcoming discussion, the electrode connected to the current amplifier is defined as the source and the electrode set to potential is defined as the drain. Figure 1 illustrates the I_S measurement relative to a common ground while V_D, V_{BG}, and V_{TG} are set relative to this common ground. In this scheme the second probe acts as the contact to the drain, and the chuck is connected to the back gate, while the conductive AFM tip is acting as a mobile nanoscaled top gate. The contact area of the highly doped full-diamond tip is estimated to be 100 nm^2.

The position and orientation of the SiNWSBFET were acquired by scanning electron microscopy (SEM) and AFM. SEM analysis shows silicidation at both NW ends, resulting in abrupt interfaces and therefore sharp Schottky junctions. Moreover, a second SEM analysis in Fig. 2(a), done after SGM measurement, yields an intact NW, showing that SGM has not damaged the NW. The AFM

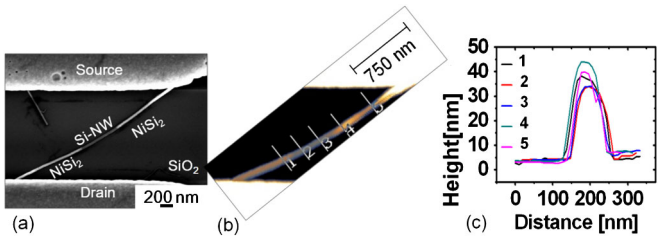

FIG. 2 (color online). (a) SEM micrograph of the NW. Source and drain Ni contacts are visible on the top and bottom of the image. The $NiSi_2$ parts of the NW are brighter than the Si part. Another nanowire on the top left is not contacted to both electrodes and therefore not the subject of this work. (b) AFM topography map of the same NW. (c) Profiles 1–5 correspond to the positions in (b) and show different diameters.

topography map in Fig. 2(b) matches the SEM micrograph. The NW appears broader due to the fact that the AFM map is the convolution of the AFM tip shape and the sample surface. The difference between the Si and $NiSi_2$ segments is also visible. This is the result of the increased NW diameter depicted by the profiles in Fig. 2(c). Profiles 2 and 3 are taken of the Si NW, and 1, 4, and 5 are taken at the $NiSi_2$ source and drain. Based on this finding, it is possible to locate the exact position of the junction in AFM morphology maps.

The device was thereafter characterized electrically in a shielded probe station using a semiconductor characterization system. The transfer characteristics were measured by contacting the source, drain, and back gate, the latter via the probe station chuck. First, a drain bias of $V_D = -1.0$ V was applied, and the back gate bias (V_{BG}) was swept between -3.0 and 3.0 V while monitoring the drain current I_D. The transfer characteristics acquired in the probe station and shown in Fig. 3(a) exhibit a clear p-type transistor behavior [8]. This p-type behavior in an intrinsic Si NW is explained by holes being injected more effectively through the Schottky junction than electrons [9]. Figure 3(b) depicts schematically how conduction and valence bands are fixed at the metallurgical junction and bent by the electric field induced by back gate bias voltage. This enables hole injection at the left Schottky junction [6,14,26]. The on-off ratio is 6 orders of magnitude. To verify the similarity of the SGM setup and the conventional testing setup, this

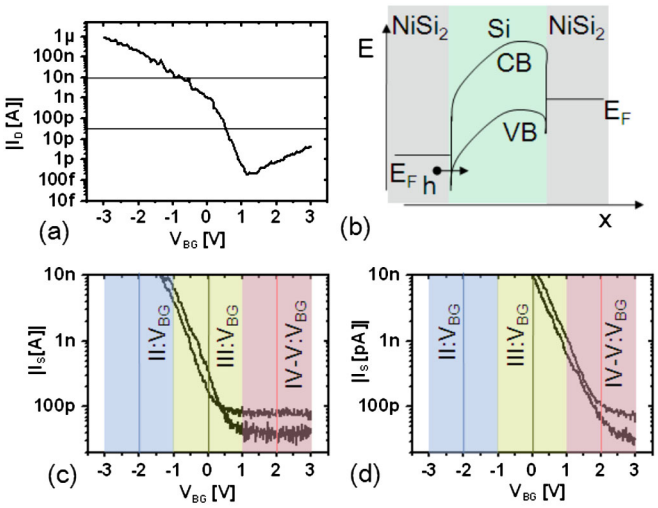

FIG. 3 (color online). (a) Transfer characteristics of the SiNWSBFET with $V_D = -1$ V measured on a probe station. The horizontal lines mark the current range of the SGM setup. (b) Band diagram schematic of hole tunneling through the Schottky junction at an applied back gate bias. (c),(d) The transfer characteristics measured in the SGM setup under the same conditions before and after SGM. The shaded areas mark the gate bias range affected by the top gate bias during the corresponding SGM measurement (II–V) at the V_{BG} marked by the corresponding line.

experiment was repeated in the SGM. Here, V_D was set to -1.0 V. V_{BG} was swept between -3.0 and 3.0 V. The transfer characteristics acquired in the SGM setup [Fig. 3(c)] without an active top gate comply with the ones acquired in the probe station, with respect to the different current measurement. The amplifier reaches its current limit at 10 nA. Figure 3(d) shows the transfer characteristics measured after SGM measurements. The device still shows switching behavior. The shift in the curves might be due to measurement in ambient conditions and slight surface manipulation by the biased tip. Afterwards, the AFM tip was set on the sample surface and scanning began. The source current was constantly monitored during scanning. In this way, a rupture of the NW, caused by the scanning motion of the AFM tip, can be detected immediately. But more importantly, any perturbation of the on or off state of the device by the scanning top gate could be detected. The nanoscopic electrical properties of the NW were examined by repeatedly scanning the NW at different top and back gate biases. The scan direction is always parallel to the NW to minimize mechanical stress. The first SGM current map was acquired at $V_D = -1.0$ V, $V_{BG} = -1.0$ V, and $V_{TG} = 1.0$ V.

In Fig. 4, SGM morphology and current maps yield a correlation between the location of the source Schottky junction and an area of high positive current. Currents at the source Schottky junction cannot be observed. Only at some sites at the silicide segment's facets can leakage currents be observed (see the inset). Here, the native oxide

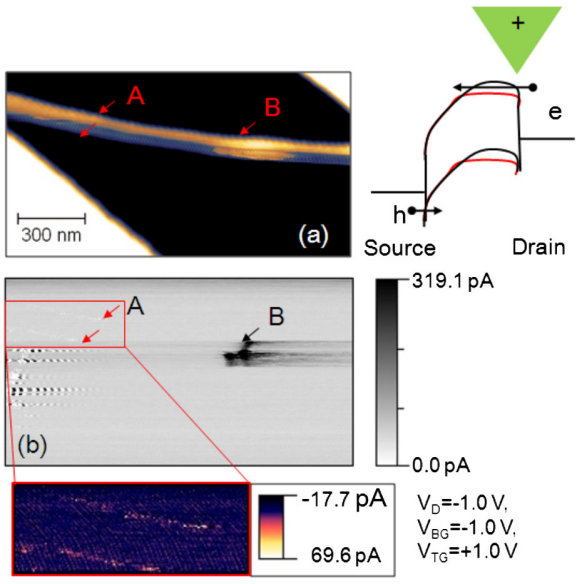

FIG. 4 (color online). (a) Topography map of the Si NW. The slight distortion of the NW is caused by the NW being moved by the tip. (b) Current map of the same area. The area marked with a red rectangle was enlarged and contrast was adjusted to display negative currents. The band diagram schematically depicts local band bending with just the back gate in black and with the additional top gate over the right Schottky junction in red.

is penetrated due to the excessive force between the tip and Ni or $NiSi_2$-NW edge during scanning. These leakage currents are significantly lower in absolute value compared to currents at the source Schottky junction and of opposite sign. Moreover, there are artifacts of high noisy currents when the AFM tip connects with the left (source) Ni electrode which is directly connected to the amplifier. The switching into the on state of the device when the biased tip is above the right Schottky junction is caused by highly local band bending of the Si conduction and valence bands. The band diagram sketch next to the current map illustrates the role of localized band bending induced by the top gate in carrier transport. In the case of a positively biased tip as in Fig. 4(b), where the tip is above the right Schottky junction, the electric field of the tip pushes the conduction and valence bands down locally at the Schottky junction. Electrons can now be injected through the right barrier and contribute to the current in addition to the holes tunneling through the left Schottky junction. Afterwards, the source and drain contact were interchanged. Again a SGM current map was acquired at different V_D, V_{BG}, and V_{TG}.

To verify the transistor symmetry, further SGM morphology and current maps, with interchanged source and drain, are shown in Fig. 5(a). Again the device is switched into the on state when the tip is on top of the drain junction. In Fig. 5(b), at $V_{BG} = 0$ V, the current is also increased when the AFM tip is just on top of the drain Schottky junction, indicating that band banding is similar to Fig. 5(a). In Fig. 5(c), at $V_{BG} = 2.0$ V, the AFM tip also pushes down the bands at the drain Schottky junction when the tip is directly on top of the junction, indicating that electrons are still the main contributor of current at the Schottky junction. These results show that electron injection via the top-gated Schottky junction dominates and that the device is symmetric. In Fig. 5(d), the top gate bias is negative and the source Schottky junction is visible for a few scan lines (see the red arrow); this on state persists throughout the rest of this image acquisition. In fact, it persists even for the following images and is showing larger positive currents than the current maps [(a)–(c)]. The drain Schottky junction is no longer visible. When the tip is positioned above the source Schottky barrier, the conduction and valence bands are pushed up and now the hole current is added to the electron current resulting in an increased total current. After a few scan lines, the transistor switches to a permanent on state. This effect lasts for the entire scan, resulting in large currents for the remainder of the current map. Moreover, this behavior is persistent throughout the following current maps when image acquisition parameters remain unchanged. The negative tip induces a negatively charged layer in the native oxide which has the same effect as the biased top gate. Accordingly, the transistor behavior can be programmed in a nonvolatile manner by charging the SiO_2 above the Schottky junction.

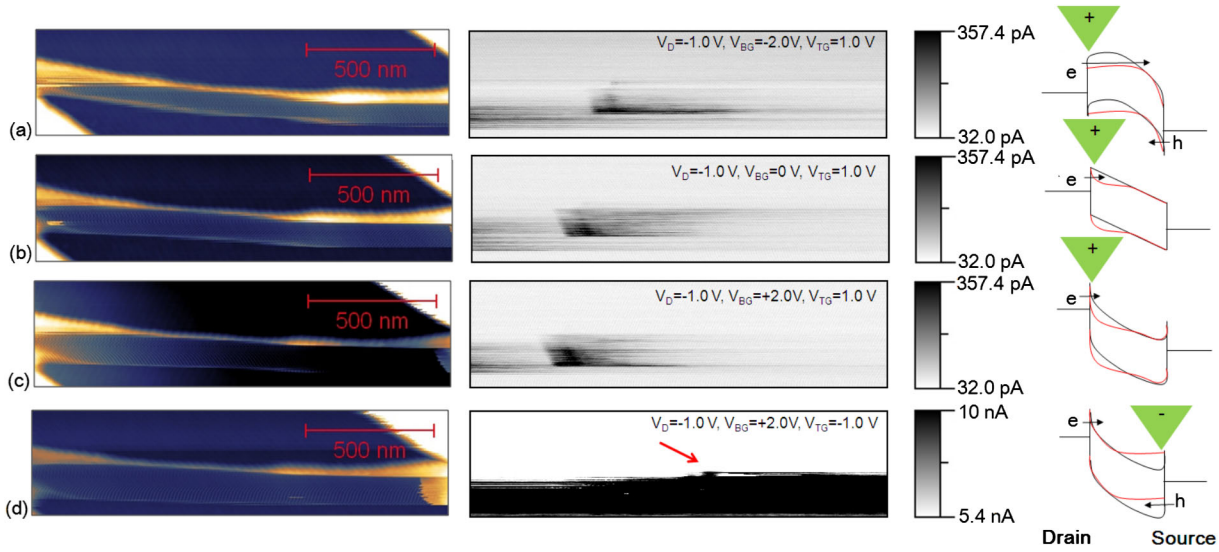

FIG. 5 (color online). SGM maps after interchanging the source and drain. Left: Topography map of the Si NW. Right: Current map of the corresponding area. The band diagrams schematically depict the band bending with just a BG (black) and with an additional TG (red) over the corresponding Schottky junction.

After changing image acquisition parameters, the original *p*-type transistor behavior is achieved again as depicted in Fig. 3(d). This result is a proof of concept for a nonvolatile memory device based on local band bending induced by charges trapped in a functionalized oxide layer above the Schottky junction.

By proving that the Schottky junctions are the area most sensitive to a local electric field, these results are of considerable insight into charge carrier transport mechanisms in metal-semiconductor junctions in general, for example, in carbon nanotubes and graphene ribbons. These findings yield more specific implications on the optimization of biosensors based on SiNWSBFET. In these nanodevices, receptors are typically placed directly above the active region where they can bind charged target biomolecules, shifting the threshold voltage [27]. Our results show that the optimal placement of receptors in nanowire SBFET biosensors is in the direct vicinity of the Schottky junctions due to their high sensitivity to electric fields.

In conclusion, scanning gate microscopy was employed to prove that the Schottky junctions control the charge carrier transport in nanometer-scale Schottky FETs. Moreover, it was demonstrated that it is possible to program the conductance of a SiNWSBFET in a nonvolatile manner by charging the oxide directly at the Schottky junction.

*dominik.martin@namlab.com

[1] M. Diarra, Y. M. Niquet, C. Delerue, and G. Allan, Phys. Rev. B **75**, 045301 (2007).
[2] M. Björk, H. Schmid, J. Koch, H. Riel, and W. Riess, Nature Nanotech. **4**, 103 (2009).
[3] Y. Nishi, U.S. Patent No. 587 527 (1970).
[4] M. P. Lepselter and S. M. Sze, Proc. IEEE **56**, 1400 (1968).
[5] S. J. Tans, A. R. M. Verschueren and C. Dekker, Nature (London) **393**, 49 (1998).
[6] J. Appenzeller, M. Radosavljevic, J. Knoch, and P. Avouris, Phys. Rev. Lett. **92**, 048301 (2004).
[7] X. Wang, Y. Ouyang, X. Li, H. Wang, J. Guo, and H. Dai, Phys. Rev. Lett. **100**, 206803 (2008).
[8] Y. Cui, X. Duan, J. Hu, and C. M. Lieber, J. Phys. Chem. B **104**, 5213 (2000).
[9] J. M. Larson and J. P. Snyder, IEEE Trans. Electron Devices **53**, 1048 (2006).
[10] J. Kedzierski, P. Xuan, E. H. Anderson, J. Bokor, Tsu-Jae King, and Chenming Hu, in *Proceedings of the International Electron Devices Meeting 2000*, IEDM Technical Digest (IEEE, New York, 2000), p. 57.
[11] F. Leonard and A. A. Talin, Phys. Rev. Lett. **97**, 026804 (2006).
[12] F. Leonard, A. A. Talin, B. S. Swartzentruber, and S. T. Picraux, Phys. Rev. Lett. **102**, 106805 (2009).
[13] J. Knoch and J. Appenzeller, Appl. Phys. Lett. **81**, 3082 (2002).
[14] W. M. Weber, L. Geelhaar, F. Kreupl, H. Riechert, L. Lamagna, M. Fanciulli, G. Scarpa, and P. Lugli, in *Proceedings of the IEEE Conference on Nanotechnology* (IEEE, New York, 2008), Vol. 244, p. 580.
[15] H. Yan, H. S. Choe, S. W. Nam, Y. Hu, S. Das, J. F. Klemic, J. C. Ellenbogen, and C. M. Lieber, Nature (London) **470**, 240 (2011).
[16] S. Zhang, H. Wei, K. Bao, U. Hakanson, N. J. Halas, P. Nordlander, and H. Xu, Phys. Rev. Lett. **107**, 096801 (2011).
[17] H. Wei, Z. Li, Z. Wang, F. Cong, N. Liu, S. Zhang, P. Nordlander, Naomi J. Halas, and H. Xu, Nano Lett. **11**, 471 (2011).
[18] Jun Hu, Yang Liu, C. Z. Ning, R. Dutton, and Sung-Mo Kang, Appl. Phys. Lett. **92**, 083503 (2008).

[19] M. Freitag, M. Radosavljevic, Y. Zhou, W. F. Smith, and A. T. Johnson, Appl. Phys. Lett. **79**, 3326 (2001).
[20] B. Tian, P. Xie, T. J. Kempa, D. C. Bell, and C. M. Lieber, Nature Nanotech. **4**, 824 (2009).
[21] M. S. Gudiksen, L. J. Lauhon, J. Wang, D. Smith, and C. M. Lieber, Nature (London) **415**, 617 (2002).
[22] Y. Wu, J. Xiang, C. Yang, and C. M. Lieber, Nature (London) **430**, 61 (2004).
[23] R. S. Wagner and W. C. Ellis, Appl. Phys. Lett. **4**, 89 (1964).
[24] W. M. Weber, L. Geelhaar, A. P. Graham, E. Unger, G. S. Duisberg, M. Liebau, W. Palmer, C. Cheze, H. Riechert, P. Lugli, and F. Kreupl, Nano Lett. **6**, 2660 (2006).
[25] K. C. Lu, W. W. Wu, H. W. Wu, C. M. Tanner, J. P. Chang, L. J. Chen, and C. M. Tu, Nano Lett. **7**, 2389 (2007).
[26] J. Knoch, M. Zhang, J. Appenzeller, and S. Mantl, Appl. Phys. A **87**, 351 (2007).
[27] K. Chen, B. Li, and Y. Chen, Nano Today **6**, 131 (2011).